Numerical study of bifurcation solutions of spherical Taylor-Couette flow*

YUAN Li (袁 礼), FU Dexun (傅德薰) and MA Yanwen (马延文)

(LNM, Institute of Mechanics, Chinese Academy of Sciences, Beijing 100080, China)

Received August 18, 1995

Abstract The steady bifurcation flows in a spherical gap (gap ratio $\sigma=0.18$) with rotating inner and stationary outer spheres are simulated numerically for $Re_{c_1} \leqslant Re \leqslant 1500$ by solving steady axisymmetric incompressible Navier-Stokes equations using a finite difference method. The simulation shows that there exist two steady stable flows with 1 or 2 vortices per hemisphere for $775 \leqslant Re \leqslant 1220$ and three steady stable flows with 0, 1, or 2 vortices for $1220 < Re \leqslant 1500$. The formation of different flows at the same Reynolds number is related with different initial conditions which can be generated by different accelerations of the inner sphere. Generation of zero- or two-vortex flow depends mainly on the acceleratio n, but that of one-vortex flow also depends on the perturbation breaking the equatorial symmetry. The mechanism of development of a saddle point in the meridional plane at higher *Re* number and its role in the formation of two-vortex flow are analyzed.

Keywords: numerical simulation, spherical Taylor-Couette flow, non-unique solutions of N-S equations, symmetry-breaking bifurcation.

Numerous theoretical and experimental investigations have been undertaken on flows between two concentric rotating spheres for over 30 years[1—5]. These flows exhibit typical nonlinear behavior when they evolve from stable laminar flows to turbulent flows as *Re* number increases. They are similar to Taylor-Couette flows in finite-length cylinders, yet are purer because they are free from end-plate conditions which are difficult to treat in cylindrical Couette flows. The most frequently studied spherical Couette flow, in which the inner sphere rotates and the outer one holds stationary, has only two control parameters: Reynolds number $Re\left(Re=\frac{\Omega_1 R_1^2}{\nu}\right)$ and gap ratio $\sigma\left(\sigma=\frac{R_2-R_1}{R_1}\right)$ where the density and viscosity are constants. Different numbers of Taylor vortices will be produced if *Re* number exceeds a critical value. Each Taylor-vortex flow mode exists only in a certain range of *Re* number whereas multiple flow modes can exist at the same *Re* number within some ranges of *Re*. For example, Sawatzki[1] and Wimmer[1, 2] have observed three steady axisymmetric modes with 0, 1 or 2 vortices and two unsteady nonaxisymmtric modes with 1 or 2 vortices at supercritical *Re* numbers at a gap ratio of $\sigma=0.18$, thus validating experimentally the non-uniqueness of solutions of the N-S equations. However, there is a discrepancy between

* Project supported by the National Natural Science Foundation of China.

experimental and numerical studies with regard to the conditions needed to produce different flow modes. For example, Wimmer's experiment[2] showed that 1-vortex flow with equatorial and axial symmetry could be generated by accelerating the inner sphere from rest to its final angular velocity at an angular acceleration ($\dot{\Omega}_1=0.0065\Omega_1^2$), but Bartels' finite difference calculation[3] with equatorial symmetry conditions could not obtain 1-vortex flow by even smaller acceleration unless the position of the equator is shifted a little distance. Later, Shrauf[4] found a symmetry-breaking bifurcation point at $Re=Re_{c_1}$ in transition from 0-vortex to 1-vortex flow by a continuation method. In computing the unsteady axisymmetric N-S equations by a pseudospectral method Marcus and Turkerman[5] obtained 1-vortex flow using 1/2 domain ($0\leqslant\theta\leqslant\pi$). They also found that the generation of 1-vortex flow experienced equatorial symmetry-breaking process. But there is much to be done as to why different accelerations produce different flow modes.

Different artificial initial conditions may be used with a steady flow solver. For example, Yang[1] obtained stable 1-vortex and 2-vortex flows using only 1/4 domain ($0\leqslant\theta\leqslant\pi/2$). His method imposed one or two radial dividing lines in the initial stage of computation and removed them later. The dividing line resembles the boundary of Taylor vortices. However, the essential difference between the different artificial initial conditions is not clear.

In this paper pseudocompressibility method is utilized to solve the steady axisymmetric incompressible N-S equations, and several steady stable bifurcation flows are simulated. After adding implicit viscous terms to the left-hand-side factor, not only is numerical instability removed from low to middle *Re* number flows but also is computational efficiency enhanced compared with original LU-SGS scheme[6]. The ability to resolve vortices is improved by adopting a third-order upwind compact finite difference for convective terms. Computational results for three steady flows at $\sigma=0.18$ show that supercritical 0-vortex flow can be obtained by fast acceleration of the inner sphere, 2-vortex flow can be obtained by slower acceleration and 1-vortex flow can be obtained by much slower acceleration in the presence of perturbations that break the equatorial symmetry conditions. The routes leading to different flow modes and their mechanism are analyzed. The computed vortex size and balance torque coefficients are in good agreement with the experimental results.

1 Governing equations and numerical method

Let τ be time, p be pressure, u, v, w be velocity components in Cartesian coordinates, $\hat{Q}$ be primitive conservative variables, $\hat{E}$, $\hat{F}$ and $\hat{G}$ be inviscid flux vectors, and $\hat{E}_v$, $\hat{F}_v$ and $\hat{G}_v$ be viscous terms. The modified incompressible N-S equations with pseudocompressibility are[6]

1) Yang J K., Numerical studies of axially symmetric motion of an incompressible viscous fluid between two concentric rotating spheres. *Ph. D. dissertation*, Marquette University, 1987.

$$\frac{\partial \hat{Q}}{\partial \tau}+\frac{\partial(\hat{E}-\hat{E}_v)}{\partial \xi}+\frac{\partial(\hat{F}-\hat{F}_v)}{\partial \eta}+\frac{\partial(\hat{G}-\hat{G}_v)}{\partial \zeta}=0, \tag{1}$$

where

$$\hat{Q}=\frac{1}{J}\begin{bmatrix} p \\ u \\ v \\ w \end{bmatrix},\quad \hat{E}=\frac{1}{J}\begin{bmatrix} \beta U \\ Uu+\xi_x p \\ Uv+\xi_y p \\ Uw+\xi_z p \end{bmatrix},\quad \hat{F}=\frac{1}{J}\begin{bmatrix} \beta V \\ Vu+\eta_x p \\ Vv+\eta_y p \\ Vw+\eta_z p \end{bmatrix},\quad \hat{G}=\frac{1}{J}\begin{bmatrix} \beta W \\ Wu+\zeta_x p \\ Wv+\zeta_y p \\ Ww+\zeta_z p \end{bmatrix}.$$

Here β is pseudocompressibility factor, U, V, W are contravariant velocities, and J is the Jacobian of coordinate transformation. The viscous terms for laminar flows are

$$\hat{E}_v=\frac{1}{ReJ}\begin{bmatrix} 0 \\ (\nabla\xi\cdot\nabla\xi)u_\xi+(\nabla\xi\cdot\nabla\eta)u_\eta+(\nabla\xi\cdot\nabla\zeta)u_\zeta \\ (\nabla\xi\cdot\nabla\xi)v_\xi+(\nabla\xi\cdot\nabla\eta)v_\eta+(\nabla\xi\cdot\nabla\zeta)v_\zeta \\ (\nabla\xi\cdot\nabla\xi)w_\xi+(\nabla\xi\cdot\nabla\eta)w_\eta+(\nabla\xi\cdot\nabla\zeta)w_\zeta \end{bmatrix},$$

$$\hat{F}_v=\frac{1}{ReJ}\begin{bmatrix} 0 \\ (\nabla\eta\cdot\nabla\xi)u_\xi+(\nabla\eta\cdot\nabla\eta)u_\eta+(\nabla\eta\cdot\nabla\zeta)u_\zeta \\ (\nabla\eta\cdot\nabla\xi)v_\xi+(\nabla\eta\cdot\nabla\eta)v_\eta+(\nabla\eta\cdot\nabla\zeta)v_\zeta \\ (\nabla\eta\cdot\nabla\xi)w_\xi+(\nabla\eta\cdot\nabla\eta)w_\eta+(\nabla\eta\cdot\nabla\zeta)w_\zeta \end{bmatrix},$$

$$\hat{G}_v=\frac{1}{ReJ}\begin{bmatrix} 0 \\ (\nabla\zeta\cdot\nabla\xi)u_\xi+(\nabla\zeta\cdot\nabla\eta)u_\eta+(\nabla\zeta\cdot\nabla\zeta)u_\zeta \\ (\nabla\zeta\cdot\nabla\xi)v_\xi+(\nabla\zeta\cdot\nabla\eta)v_\eta+(\nabla\zeta\cdot\nabla\zeta)v_\zeta \\ (\nabla\zeta\cdot\nabla\xi)w_\xi+(\nabla\zeta\cdot\nabla\eta)w_\eta+(\nabla\zeta\cdot\nabla\zeta)w_\zeta \end{bmatrix}.$$

Backward Euler difference is applied to the time derivatives; fluxes at time level $n+1$ are linearized with respect to time level n and spatial difference approximations are introduced. We obtain equations of delta form

$$[I+\Delta\tau(D_\xi\hat{A}+D_\eta\hat{B}+D_\zeta\hat{C})]^n\,\delta\hat{Q}=RHS^n$$
$$=-\Delta\tau[D_\xi(\hat{E}-\hat{E}_v)+D_\eta(\hat{F}-\hat{F}_v)+D_\zeta(\hat{G}-\hat{G}_v)]^n, \tag{2}$$

where I is identity matrix, $\delta\hat{Q}=\hat{Q}^{n+1}-\hat{Q}^n$, D_ξ, D_η and D_ζ are finite difference operators approximating ∂_ξ, ∂_η, and ∂_ζ, $\hat{A}$, $\hat{B}$ and $\hat{C}$ are inviscid Jacobian matrices.

We use lower-upper symmetric Gauss-Seidel scheme[6] to solve (2), whose formula is

$$LD^{-1}U\delta\hat{Q}=RHS^n, \tag{3}$$

where

$$\begin{cases} L=I+\Delta\tau(\nabla_\xi\hat{A}^+ +\nabla_\eta\hat{B}^+ +\nabla_\zeta\hat{C}^+ -\hat{A}^- -\hat{B}^- -\hat{C}^-), \\ D=I+\Delta\tau(\hat{A}^+ +\hat{B}^+ +\hat{C}^+ -\hat{A}^- -\hat{B}^- -\hat{C}^-), \\ U=I+\Delta\tau(\Delta_\xi\hat{A}^- +\Delta_\eta\hat{B}^- +\Delta_\zeta\hat{C}^- +\hat{A}^+ +\hat{B}^+ +\hat{C}^+). \end{cases} \tag{4}$$

To attain scalar inversion, Jacobian matrix may be constructed using approximate matrix:

$$\begin{cases} \hat{A}^\pm = \dfrac{1}{2}[\hat{A}\pm\rho(\hat{A})I], \\ \rho(\hat{A})=\kappa\max[|\lambda(\hat{A})|], \end{cases} \tag{5}$$

where $\lambda(\hat{A})$ is eigenvalue of Jacobian matrix $\hat{A}$ and their formulae are given in ref. [6]. We take $\kappa=1$ instead of $\kappa\geqslant 1$ in ref. [6]. The original LU-SGS scheme is unstable to middle Re number flows because it does not include implicit viscous terms. Our version retains orthogonal implicit viscous terms and the Jacobian matrix in (4) is modified as

$$\hat{A}^\pm = \frac{\hat{A}\pm\rho(\hat{A})I}{2} \pm \frac{\alpha}{2} I_m, \tag{6}$$

where $\alpha=\gamma_1=\dfrac{1}{Re}\nabla\xi_i\cdot\nabla\xi_i$, $I_m=\mathrm{diag}(0,\ 1,\ 1,\ 1)$.

For the first-order derivatives of convective terms in the RHS of (3), the third-order upwind compact finite difference[7] is applied. The upwinding is constructed according to the sign of eigenvalues of inviscid Jacobian matrix. We take ξ direction as an example:

$$D_\xi\hat{E}=AD_\xi Q=A^+F^+(Q)+A^-F^-(Q), \tag{7}$$

where $A^\pm=T_\xi\Lambda_\xi^\pm T_\xi^{-1}$. The third-order compact finite difference is computed by

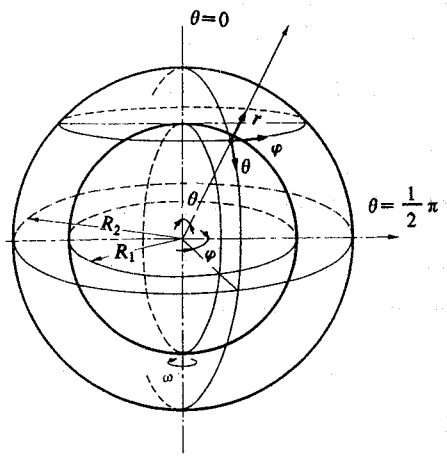

Fig. 1. Geometry definition of a spherical gap.

$$\begin{cases} \dfrac{1}{3}(2F_i^+ +F_{i-1}^+)=\dfrac{1}{6\Delta\xi}(-5Q_{i-1}+4Q_i+Q_{i+1}), \\ \dfrac{1}{3}(2F_i^- +F_{i+1}^-)=\dfrac{1}{6\Delta\xi}(5Q_{i+1}-4Q_i-Q_{i-1}). \end{cases} \tag{8}$$

The derivatives next to the boundaries are approximated by the third-order biased finite difference.

For the concentric spherical annulus shown in fig. 1, two computational domains, $1/4(0\leqslant\theta\leqslant\pi/2)$ and $1/2(0\leqslant\theta\leqslant\pi)$ are used. In the former case, equatorial symmetry conditions at $\theta=\pi/2$ are imposed while in the latter case asymmetric numeri-

cal perturbations are allowable. All boundary conditions are treated explicitly. Non-slip condition is applied to velocities, and the pressure is obtained by the momentum equation in radial direction on both spheres. Axial symmetry conditions are applied to poles and a reference pressure is taken at a specified point in the interior domain.

2 Initial conditions and routes to supercritical non-unique flow modes

Two kinds of initial conditions are used in this study, one is that obtained by accelerating the inner sphere at different angular accelerations from rest to an angular velocity corresponding to a steady *Re* number; the other is the same as that of Yang's linear velocity profile across the gap in the azimuthal direction, with zero velocity components in the meridional plane and zero static pressure in the whole domain with the imposition of one or several radial dividing lines. The former is used for studying the influence of the accelerations and for comparison with experiments while the latter is mainly for comparison with Yang's results. Numerous experiments and numerical simulations have confirmed that for supercritical *Re* numbers, faster acceleration yields 0-vortex flow, slower acceleration gives rise to 2-vortex flow and much slower acceleration under no equatorial symmetry restriction gives 1-vortex flow. However, experiments differ significantly from numerical computations in the range of accelerations to obtain a flow mode. It may be expected that symmetry imperfections are frequently caused in experiments by eccentricity of two spheres and leakage between the rotating axis and spherical shells and they will result in larger equatorial or axial nonsymmetric disturbances, hence easily promoting symmetry-breaking instability under the influence of nonlinearity. We know that each steady flow at supercritical *Re* numbers is a branch of bifurcation solutions of N-S equations and it exists only within a limited range of control parameters. A bifurcation solution also depends on the initial conditions. The role of angular acceleration is to produce different initial conditions. In the next paragraph we give an explanation why different angular accelerations produce different initial flowfields of a particular Taylor-vortex flow.

We first cite the torque-*Re* curve of Marcus and Tuckerman[5] to identify different ranges of *Re* number for several Taylor-vortex flows to exist (fig. 2). There is only stable 0-vortex flow for $0 \leqslant Re \leqslant 645$ and both 0-vortex and 2-vortex flows are linearly unstable for $651 \leqslant Re \leqslant 775$ without equatorial symmetry restriction. Therefore, only 1-vortex flow can be stable in this *Re*-range. 1-vortex and 2-vortex flows can exist at $Re \geqslant 775$ and our simulation further shows that supercritical

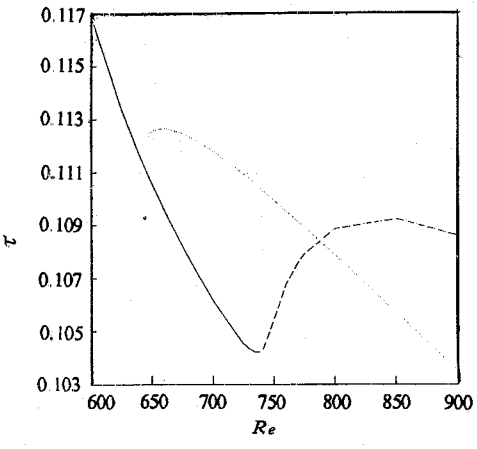

Fig. 2. Torque-*Re* curve computed by Marcus[5]. Solid line, 0-vortex; dotted line, 1-vortex; dashed line, 2-vortex flow

0-vortex flow becomes stable only after $Re \geqslant 1\,220$. Now let the final Re number be greater than 1 220. The inertia of fluid makes its evolution lag behind when the inner sphere is accelerated from rest to this Re number. No matter how great the acceleration is, the flow will certainly pass by a low Re number stage. In fact, the centrifugal force makes the fluid develop into a secondary flow in the meridional plane as soon as the inner sphere begins to rotate, which looks like a 0-vortex flow. If the angular acceleration is large, the instant Re number quickly reaches its final value shortly after 0-vortex flow is produced, hence a 0-vortex initial flowfield is obtained from which steady 0-vortex flow develops; if the acceleration is small, the instant Re number still quickly passes through the range $651 \leqslant Re \leqslant 775$ and nonsymmetric disturbance has no time to grow; yet the instant Re number halts for enough time above 775 and the total circulation continues to increase making the flow develop toward 2-vortex flow. When Re number reaches its final value, 2-vortex initial flowfield is formed from which stable 2-vortex flow develops. If the accleration is so small that the instant Re number halts for a long time within $651 \leqslant Re \leqslant 775$, any small asymmetric disturbance will be amplified to the extent that nonlinearity will play a certain role in destabilizing the flow, in this way 1-vortex initial flowfield is formed from which stable 1-vortex flow develops. Such a transition to 1-vortex flow can by no means be realized only by reducing acceleration if equatorial symmetry restriction is imposed. In this case 1-vortex flow may be obtained by artificially assuming a 'crude' 1-vortex flow according to the dependence of bifurcation solutions on the initial conditions. The inflow at the equator is an essential feature of 1-vortex flow. In the initial stage of computation, an artificial radial dividing line is set near the equator, and symmetry condition is used on this line, then the fluid moves outward along it. However, the fluid at the equator moves inward, as can be expected from continuity equation. A rough 1-vortex flow is thus produced between the equator and the artificial dividing line. After this line is removed, the flow settles down toward 1-vortex flow if Re is above Re_{c_1}. Although it is the case with computation, it is not realizable in experiments where asymmetric perturbations play an essential role. Let us see how the asymmetric disturbance affects the bifurcation.

Because both geometry and the known steady stable flows are symmetric with respect to the equator, any small disturbance with respect to each base flow, according to linear stability theory, can be disintegrated as two eigenmodes: one symmetric and the other antisymmetric about the equator. Both modes satisfy the linearized evolution equation, and for any Re number and wave number, both modes have different growth or damping rates. 0-vortex and 2-vortex flows are linearly unstable and 1-vortex flow is linearly stable for $651 \leqslant Re \leqslant 775$ (see fig. 2). Ref. [5] further showed that this instability is that of antisymmetric eigenmode. It is evident that the range $651 \leqslant Re \leqslant 775$ is an attraction region of 1-vortex flow, for any small asymmetric disturbance to 0- or 2-vortex flow will grow to the extent for nonlinearity to act. Previous studies and our numerical simulations show that other flows first develop into a nonsymmetric intermediate state and then recover to

symmetric 1-vortex flow. Such a transition is termed symmetry-breaking bifurcation. The necessary nonsymmetric disturbance may be easily produced in experiments and numerical simulations when 1/2 domain is used. Our simulation further indicates that symmetry-breaking instability grows so slowly and in so narrow a range $651 \leqslant Re \leqslant 775$ that it is necessary to accelerate the inner sphere very slowly in order to keep the instant Re number within the range.

To sum up, we have found two routes leading to stable bifurcation solutions at supercritical Re numbers. In the former, the acceleration is changed from large to small, yielding 0-vortex, 2-vortex to 1-vortex flow. In the latter, artificial dividing lines are imposed for a Taylor-vortex flow to develop within a certain range of Re number. In the two routes the dependence of bifurcations on the initial conditions is utilized.

3 Computed results and discussions

In the present computation, grid number is $21(r) \times 129(\theta)$ for 1/2 domain and 21×65 for 1/4 domain. The case with $\sigma = 0.18$ and $Re \leqslant 1\,500$ is considered. Increment of Re is 100 generally or 10 for $1\,150 \leqslant Re \leqslant 1\,230$. Attention is focused on steady stable bifurcation flows at $Re \geqslant Re_{c_1} = 645$. So only two typical cases of $Re = 800$ and $Re = 1\,500$ are discussed.

3.1 $Re = 800$

If the computation domain is 1/4 annulus, only stable 2-vortex flow can be generated independently. Fig. 3 depicts the history from rest to 2-vortex flow. The flow in fig. 3 (a) is 0-vortex flow while those in figs. 3 (b) and 3 (c) are pinched flows with a saddle point S and the final state is stable 2-vortex flow (fig. 3 (e)). There is a boundary between two vortices on which the fluid flows toward the inner sphere, forming a sink on the outer sphere. The fluid at the equator flows outward, serving as a source on the outer sphere. For a pinched flow (figs. 3(b)) and 3(c)), Marcus and Turkerman indicated that the flow between the equator and the saddle point has strong coupling between meridional and azimuthal velocity components and redistributes angular momentum just as Taylor vortex does, but they did not explain why the saddle point is generated. We studied the streamfunction, velocity vector and kinematic energy in the meridional plane and found that the saddle point always develops near the center of the secondary flow, where θ-velocity component is larger and there is a shear flow generated by the flow toward the equator along the inner sphere and the flow toward the pole along the outer sphere. When Re number is increased, the shear flow becomes stronger owing to larger θ-velocity gradient and a saddle point is generated. This stagnation point is associated with higher pressure and lower kinematic energy (fig. 3(c)), so the secondary flow separates on both spheres to form two recirculation vortices. But the separation only results in kinematic change in the meridional plane. When the gap is narrow, two recirculation vortices get connected to

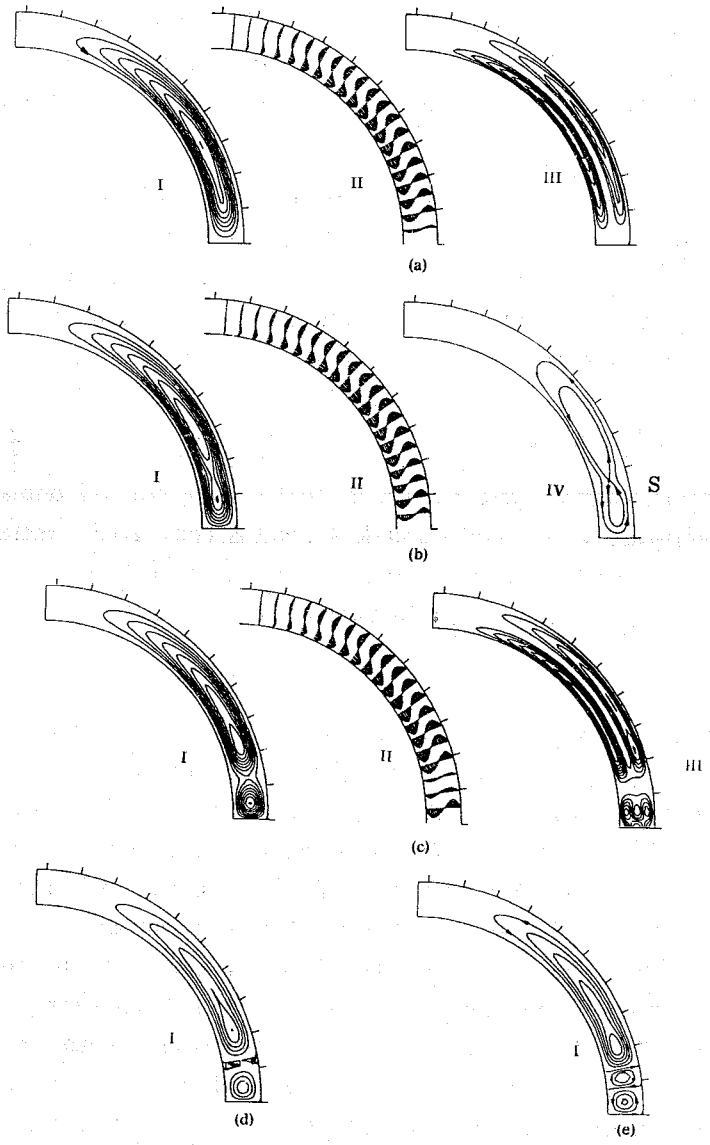

Fig. 3. Evolution from rest to 2-vortex flow. $Re=800$, $\sigma=0.18$. (I) Contours of meridional streamfunction; (II) meridional velocity vector; (III) meridional kinematic energy $q=(u^2+v^2)/2$; (IV) sketch of a saddle point. (a) 400 steps; (b) 600 steps; (c) 1 000 steps; (d) 1 230 steps; (e) 8 000 steps.

form a further one of 2-vortex flow (fig. 3(d)). Thus we see the saddle point plays an intermediary role in the formation of 2-vortex flow.

With an artificial dividing line imposed at a distance σ from the equator in the first 300 computational steps, we obtain 1-vortex flow using 1/4 domain. Fig. 4 depicts

1-vortex flow obtained in this way. However, with two artificial lines, the flow converges to 2-vortex flow. This is consistent with the result of Yang's. We imposed 3 dividing lines, but only 1-vortex flow is obtained. We see a common feature in 1 or 3 lines is that the fluid at the equator is allowed to flow toward the inner sphere, which is an essential characteristic of 1-vortex flow. The above example demonstrates the dependence of bifurcations on the initial conditions and an important discriminator between 1-vortex and 0- or 2-vortex flows.

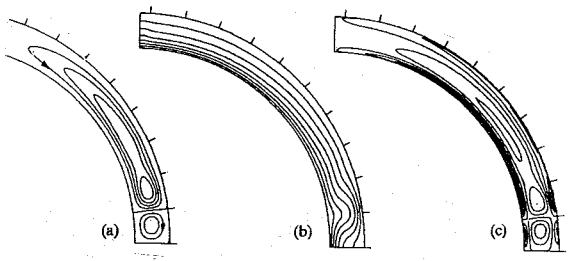

Fig. 4. Steady 1-vortex flow. $Re=800$. (a) Contours of meridional streamfunction; (b) azimuthal angluar velocity $\Omega=\frac{w}{r\sin\theta}$; (c) azimuthal vorticity component.

One-vortex flow may also be produced using 1/2 domain. If the inner sphere is accelerated from rest to $Re=800$ at $\Delta t=0.025$ within 20 000 steps, the flow evolves into 1-vortex flow. Let Re number increase up to 1 500. Then 1-vortex flow remains stable.

3.2 $Re=1\,500$

There exist 0-, 1- and 2-vortex flows at this Re number according to Wimmer[2]. Using 1/4 annulus domain and zero initial flowfield, we obtained 0-vortex flow for an acceleration $\dot{\Omega}_1=0.014$ (fig. 5), and 2-vortex flow for $\dot{\Omega}_1=0.005$ (fig. 6). Using 1/2 annulus domain, we obtained 1-vortex flow for an acceleration $\dot{\Omega}_1=0.0005$ (fig. 7). This confirms the argument of previous studies. The torque coefficients for the three flows are 0.144, 0.166 and 0.177, respectively and the vortex size of 1-vortex flow in the circumferential direction is 1.35σ. These values are within 5% uncertainty compared with the experimental[2].

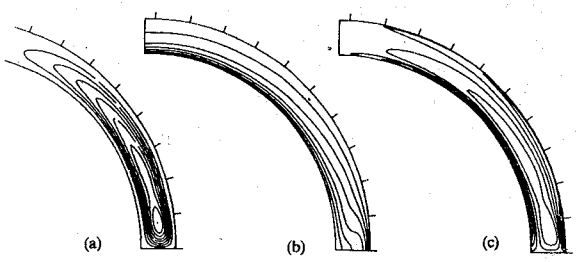

Fig. 5. Steady 0-vortex flow. $Re=1\,500$. (a) Contours of meridional streamfunction; (b) azimuthal angluar velocity $\Omega=\frac{w}{r\sin\theta}$; (c) azimuthal vorticity component.

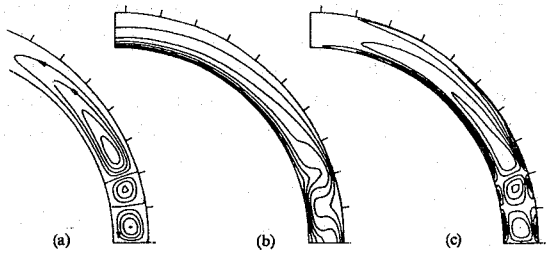

Fig. 6. Steady 2-vortex flow. $Re=1\,500$. (a) Contours of meridional streamfunction; (b) azimuthal angluar velocity $\Omega=\frac{w}{r\sin\theta}$; (c) azimuthal vorticity component.

4 Conclusions

The non-unique Taylor-Couette flows are simulated by solving the steady axisymmetric

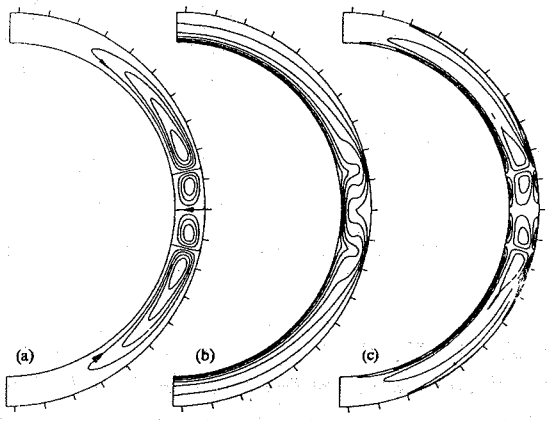

Fig. 7. Steady 1-vortex flow computed using domain $0 \leqslant \theta \leqslant \pi/2$. $Re = 1\,500$. (a) Contours of meridional streamfunction; (b) azimuthal angluar velocity $\Omega = \frac{w}{r\sin\theta}$; (c) azimuthal vorticity component.

incompressible N-S equations using a finite difference method. The computed results are in good agreement with the experimental. The mechanism of the formation of a saddle point in the meridional plane and its role in the formation of 2-vortex flow are elucidated. The importance of control parameters and angular acceleration in the flow bifurcation is analyzed. It is shown that 2-vortex flow is produced through flow separation of the secondary flow with a saddle point and the transition preserves equatorial symmetry. The transition is only a kinematic bifurcation. But 1-vortex flow is generated by centrifugal instability through symmetry-breaking bifurcation in which asymmetric disturbances are allowed to play an important role. Different steady flow modes can be generated using different initial conditions, indicating the dependence of bifurcations on the initial conditions after the flow loses stability.

References

1 Sawatzki, O., Zerip, J., Das Stromfeld im Spalt zwichen zwei konzentrischen Kulgelflachen, von denen die innere rotiert, *Acta Mechanica*, 1970, 9:13.
2 Wimmer, M., Experiments on a viscous fluid flow between concentric rotating spheres, *J. Fluid Mech.*, 1976, 78:317.
3 Bartels, F., Taylor vortices between two-concentric rotating spheres, *J. Fluid Mech.*, 1982, 119:1.
4 Schrauf, G., The first instability in spherical Taylor-Couette flow, *J. Fluid Mech.*, 1986, 166:287.
5 Marcus, P., Tuckerman, L. S., Simulation of flow between concentric rotating spheres, *J. Fluid Mech.*, 1987, 185:1.
6 Yoon, S., Kwak, D., Three-dimensional incompressible Navier-Stokes solver using Lower-Upper Symmetric Gauss-Seidel algorithm, *AIAA J.*, 1991, 29:874.
7 Liu Hong, Fu Dexun, Ma Yanwen, Upwind compact method and direct numerical simulation of driven flow in a square cavity, *Science in China*, Ser. A, 1993, 36(11):1 347.